© 2020. Published by The Company of Biologists Ltd | Journal of Cell Science (2020) 133, jcs239855. doi:10.1242/jcs.239855

RESEARCH ARTICLE

LAX28 is required for the stable assembly of the inner dynein arm f complex, and the tether and tether head complex in *Leishmania* flagella

Tom Beneke, Katherine Banecki, Sophia Fochler and Eva Gluenz*

ABSTRACT

Motile eukaryotic flagella beat through coordinated activity of dynein motor proteins; however, the mechanisms of dynein coordination and regulation are incompletely understood. The inner dynein arm (IDA) f complex (also known as the I1 complex), and the tether and tether head (T/TH) complex are thought to be key regulators of dynein action but, unlike the IDA f complex, T/TH proteins remain poorly characterised. Here, we characterised T/TH-associated proteins in the protist *Leishmania mexicana*. Proteome analysis of axonemes from null mutants for the CFAP44 T/TH protein showed that they lacked the IDA f protein IC140 and a novel 28-kDa axonemal protein, LAX28. Sequence analysis identified similarities between LAX28 and the uncharacterised human sperm tail protein TEX47, both sharing features with sensory BLUF-domain-containing proteins. *Leishmania* lacking LAX28, CFAP44 or IC140 retained some motility, albeit with reduced swimming speed and directionality and a propensity for flagellar curling. Expression of tagged proteins in different null mutant backgrounds showed that the axonemal localisation of LAX28 requires CFAP44 and IC140, and the axonemal localisations of CFAP44 and IC140 both depend on LAX28. These data demonstrate a role for LAX28 in motility and show mutual dependencies of IDA f and T/TH-associated proteins for axonemal assembly in *Leishmania*.

KEY WORDS: *Leishmania*, Cilia, Dynein, Flagella, Motility

INTRODUCTION

Eukaryotic cilia and flagella are highly conserved structures found in organisms ranging from the unicellular green algae *Chlamydomonas* and protists, such as *Leishmania*, to specialized cells in metazoans, including humans. Even though cilia and flagella have highly conserved microtubule arrangements, structural alterations generate diversity, allowing them to exhibit different behaviours in the context of their biological function, such as signalling and motility. Dysfunctions in motile and/or non-motile cilia in humans are linked to numerous diseases collectively called ciliopathies. At least 187 ciliopathy-associated genes have been identified (Reiter and Leroux, 2017), and defects in motile cilia have been shown to cause hydrocephalus in the brain, chronic respiratory problems and male infertility (Mitchison and Valente, 2017).

Sir William Dunn School of Pathology, University of Oxford, South Parks Road, Oxford OX1 3RE, UK.

*Author for correspondence (eva.gluenz@path.ox.ac.uk)

E.G., 0000-0003-4346-8896

Received 2 October 2019; Accepted 12 December 2019

Motile axonemes typically have nine microtubule doublets, consisting of an A and B microtubule, and a central pair complex of two singlet microtubules. Dynein motor proteins arranged along the A-tubule of each doublet move along the neighbouring B-tubule, while undergoing a mechano-chemical cycle of pre- and post-power stroke conformational changes powered through the hydrolysis of ATP (Lin and Nicastro, 2018; King, 2018). Since the microtubule doublets are anchored in the basal body and connected by elastic nexin links, the dynein-driven sliding motion results in flagellar bending. What remains a topic of great interest is to understand the spatio-temporal coordination of the different dynein isoforms to generate the observed flagellar waveforms (reviewed in Lindemann and Lesich, 2010).

The axoneme is organized longitudinally in regular 96-nm repeating units. Outer dynein arms (ODAs) are homogeneously spaced every 24 nm and provide the power by determining the beat frequency. Inner dynein arms (IDAs) control size and shape of the forward and reverse ciliary bend (bend amplitude). The seven subspecies of IDAs [containing dyneins a, b, c, d, e, f (also known as I1) and g] are each uniquely positioned within the 96 nm repeat unit (Bui et al., 2012; Heuser et al., 2012). Additional complexes including the calmodulin and spoke-associated complex (CSC) (Dymek et al., 2011), the modifier of inner arms (MIA) complex (Yamamoto et al., 2013) and the nexin–dynein regulatory complex (N-DRC) (Heuser et al., 2009; Huang et al., 1982; Oda et al., 2015; Ralston and Hill, 2006) have been shown to control the function of IDAs. Radial spokes (RSP) (Barber et al., 2012; Curry et al., 1992; Diener et al., 1993; Ralston and Hill, 2006; Williams et al., 1989; Yang et al., 2006, 2004) and the central pair complex (CPC) (Adams et al., 1981; Dawe et al., 2007; Dutcher et al., 1984; Lechtreck and Witman, 2007; Oda et al., 2015) also influence the activity of IDAs either directly or indirectly.

Each IDA isoform is thought to have its own role in flagellar motility (Kato-Minoura et al., 1997; Kubo et al., 2018; Perrone et al., 1998). The IDA f complex has received particular attention as the centre of a regulatory hub thought to integrate mechano-chemical signals from the CPC, RSP and other complexes (Heuser et al., 2012). IDA f is the only IDA that contains two dynein heavy chains (DHC 1α and DHC 1β) and requires an intermediate chain and light chain complex (ICLC) for incorporation into the flagellar axoneme (Heuser et al., 2012; Perrone et al., 1998; Viswanadha et al., 2014). As highlighted in Kubo et al. (2018) the *Chlamydomonas* IDA f ICLC complex contains five light chains (LC7a, LC7b, LC8, Tctex1 and Tctex2b), one accessory subunit FAP120 and two intermediate chains IC140 and IC138 (DiBella et al., 2004a,b; Harrison et al., 1998; Hendrickson et al., 2004; Ikeda et al., 2009; Myster et al., 1997, 1999; Perrone et al., 1998; Piperno, 1990; Porter et al., 1992; Smith and Sale, 1991; Toba et al., 2011). The intermediate chains have been shown to act either as regulators

Journal of Cell Science (2020) 133, jcs239855. doi:10.1242/jcs.239855

or assembly factors for the IDA f complex. IC140 has been shown to preassemble with both heavy chains in the cytoplasm before being transported by intraflagellar transport (IFT) proteins to the distal end of a growing flagellum (Viswanadha et al., 2014), while IC138 has been proven to be an important phosphorylation switch of IDA l1, regulating the beat amplitude, sliding velocities between microtubules and the speed of bend propagation (Hendrickson et al., 2004; VanderWaal et al., 2011).

The tether and tether head complex (herein denoted T/TH) has recently emerged as a new complex linked to IDA f. It was first described in *Chlamydomonas*, where cryo-electron tomography identified the T/TH structure as a link between the A-tubule and the DHC 1α motor domain in IDA f (Heuser et al., 2012). The T/TH proteins FAP44 and its paralogue FAP43 were subsequently shown to be required for assembly of the IDA f head, but not the entire complex, and they are needed for regulating conformational changes of IDAs, as well as transferring their activity into microtubule sliding motion (Fu et al., 2018; Kubo et al., 2018; Urbanska et al., 2018).

FAP43 and FAP44 are part of a core group of 50 proteins that are conserved in organisms with motile flagella (Baron et al., 2007). The human orthologues, CFAP43 and CFAP44, have been linked to non-syndromic male infertility (Krausz et al., 2015; Okutman et al., 2018; Tang et al., 2017), and loss-of-function studies confirmed a role in motility in the protists *Trypanosoma brucei* (Coutton et al., 2018) and *Leishmania mexicana* (Beneke et al., 2019). The conserved FAP57 has also been proposed to be linked to the T/TH complex (Urbanska et al., 2018). Additional components of the T/TH complex identified to date appear to be less widely conserved, such as *Chlamydomonas* FAP244 (Fu et al., 2018), MOT7, FAP102 and Cre10.g452250 (Kubo et al., 2018).

Given that we previously found that *L. mexicana CFAP44*-knockout mutants exhibited a strong motility defect, characterized by reduced swimming speed, reduced directionality (velocity/speed) and a propensity for flagellar curling (Beneke et al., 2019) we sought to identify other *Leishmania* T/TH proteins through quantitative proteomics of flagellar skeleton preparations from *CFAP44*-null mutants (*ΔCFAP44*) and control cells. This identified a previously uncharacterized flagellar protein, LAX28. Further characterisation showed that LAX28, CFAP44 and the IDA f protein IC140 show mutual dependencies for localization to the flagellar axoneme, and loss of LAX28 causes a similar motility defect to that seen upon loss of the T/TH or IC140. Interestingly, sequence analysis identified the human protein TEX47 as a putative orthologue of LAX28, suggesting a possible role for this uncharacterised human protein in sperm motility.

RESULTS

Identification of proteins missing from *ΔCFAP44* mutants axonemes

To identify new components of the *L. mexicana* T/TH complex, attempts were made to perform immunoprecipitation (IP) experiments with CFAP44. This was unsuccessful because CFAP44 remained associated with the axoneme following cell lysis and detergent extraction, and no suitable conditions could be identified under which CFAP44 dissociated from the axoneme. CFAP44 remained associated with the axoneme in a broad range of salt concentrations, including up to 2 M LiCl, 2 M $CaCl_2$, 3.2 M KCl and 4 M NaCl (Fig. S1). This stable association was then used to ask whether there were any proteins that depended on CFAP44 for their axonemal localization by comparing the protein composition of *ΔCFAP44* mutant flagella (Beneke et al., 2019) with those of the parental Cas9 T7 cell line (Beneke et al., 2017). To enrich for flagellar skeletons, NaCl-extracted flagella (Robinson and Gull, 1991) were further purified by separating components through use of a sucrose gradient (Fig. 1A–C), as this was previously shown to reduce *Leishmania* cell body contamination (Beneke et al., 2019).

Liquid chromatography tandem mass spectrometry (LC-MS/MS) analysis of *ΔCFAP44* flagella and flagella from the *L. mexicana* Cas9 T7 parental cell line, for comparison (Fig. 1C,iv), identified a total of 1162 proteins (Fig. 1D; Table S2). Proteins in the mutant and parental samples overlapped well with those found in detergent-insoluble fractions of *L. mexicana*, analysed in Beneke et al. (2019) (Fig. 1E) and included well-characterised flagellar proteins, such as CPC, N-DRC, IDA, ODA, RSP and paraflagellar rod (PFR) proteins. Although the mechanical method for flagellum isolation employed in Beneke et al. (2019) separates the external part of the motile flagellum from the cell body, the salt-extraction protocol preserved the connection with the basal body (Robinson and Gull, 1991). Consequently, a large number of proteins associated with the basal body, flagellar attachment zone (FAZ), intraflagellar transport (IFT) and tripartite attachment complex (TAC) were also identified (Table S2), further expanding the inventory of *L. mexicana* flagellum-associated proteins.

To test for protein enrichment between the *ΔCFAP44* and parental flagella, a label-free normalized spectral index quantitation method (SINQ; Trudgian et al., 2011) was used (Tables S1 and S2). 65 proteins were exclusively identified in the parental controls cells, while 32 proteins were exclusively identified in *ΔCFAP44* mutants.

Examination of the proteins missing from the *ΔCFAP44* flagella confirmed the loss of CFAP44 itself and its close homologue CFAP43. This is consistent with observations made for deletions and mutations on the T/TH complex in *Chlamydomonas* and *Tetrahymena* (Fu et al., 2018; Kubo et al., 2018; Urbanska et al., 2018), showing co-dependence of these proteins for localisation. Unexpectedly, the *L. mexicana* IDA f intermediate chain IC140 was also completely absent from the *ΔCFAP44* flagella. Moreover, the level of the IDA heavy chains DHC 1α and DHC 1β were significantly reduced in *ΔCFAP44* mutant flagella (DHC 1α was reduced by 55.6% and DHC 1β by 61.3%), while ODA, CPC and RSP components and the main component of the PFR, PFR2, showed only small changes (Table 1; Tables S1 and S2). We confirmed depletion of IC140 from *ΔCFAP44* mutant flagella by tagging IC140 with eYFP and subsequently deleting *CFAP44* in IC140::eYFP-tagged cells (Fig. 2A). Deletion of the open reading frame (ORF) was confirmed by PCR (Fig. S2A–F). In the tagged cell line, IC140::eYFP localized to the axoneme, as expected. By contrast, it was undetectable in *IC140::eYFP ΔCFAP44* mutants, thus confirming mass spectrometry results indicating that the flagellar localisation of IC140 depends on CFAP44 in *Leishmania* (Fig. 2A).

We next focused on a hitherto uncharacterized protein that was completely absent from *ΔCFAP44* flagella (Table 1; Tables S1 and S2): LmxM.24.1310 is a hypothetical protein of 254 amino acids (molecular mass of 28,257 Da; pI 4.9), with no defined domains, which we named LAX28 (for *Leishmania* axonemal protein, 28 kDa). This proteins had been previously shown to be enriched in the *L. mexicana* flagellar proteome (Beneke et al., 2019) but had not previously been linked to T/TH or IDAs.

The axonemal localisation of LAX28 depends on *CFAP44* and *IC140*

To provide MS-independent evidence that the flagellar localization of LAX28 is dependent on CFAP44, LAX28 was tagged with

Journal of Cell Science (2020) 133, jcs239855. doi:10.1242/jcs.239855

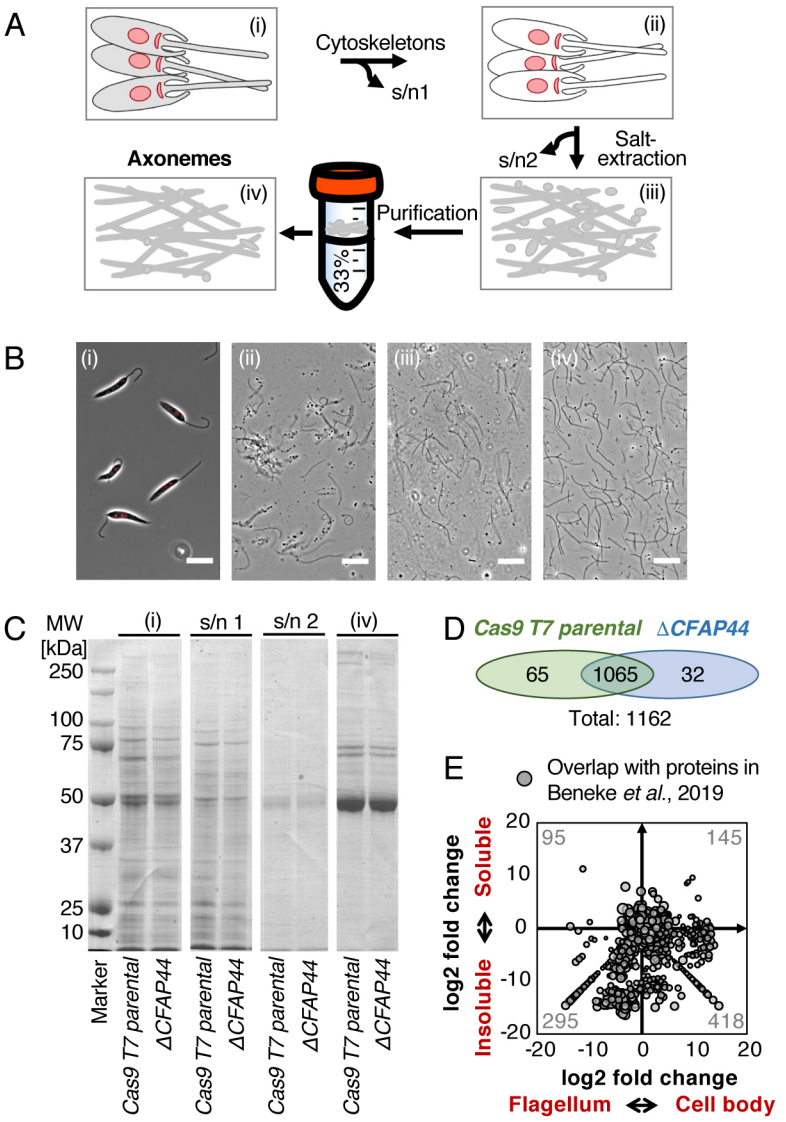

Fig. 1. Protein composition of salt-extracted *L. mexicana* flagellar axonemes. (A) Overview of the flagellar isolation protocol. Percentage sucrose concentration (w/v) and isolation of supernatants (s/n) are indicated. (B) Micrographs show merged phase and Hoechst DNA stain (red) images for each isolation stage (i–iv) depicted in A. (i) *L. mexicana* cells before detergent extraction, (ii) cells after detergent extraction, (iii) axonemes after salt extraction and (iv) isolated salt-extracted axonemes after differential centrifugation. Scale bars: 10 µm. (C) Protein gel stained with Coomassie Blue. Numbers on the left indicate molecular mass in kDa. Lane i and s/n 1 were loaded with protein from 4×10^6 cells. Protein amounts for lane i and iv are as follows: *Cas9 T7* parental (i) 2.02 µg and (iv) 0.74 µg, *ΔCFAP44* (i) 2.56 µg and (iv) 0.82 µg; 4 µg of each sample in lane iv were submitted for mass spectrometry analysis. (D) Venn diagram showing the total number of all detected proteins (≥2 peptides detected, $P>0.95$). (E) Proteins detected in salt-extracted flagella mapped onto the SINQ enrichment plot of proteins detected in N-octyl-glucoside soluble and insoluble flagellar and cell body fractions of *L. mexicana* (data from Beneke et al., 2019). Each grey dot indicates a protein detected in both studies, the number of proteins is also indicated.

mNeonGreen (mNG) and tagged cells were then subjected to deletion of *CFAP44*, *IC140*, *DRC2*, *Hydin*, *LC7*, *PF16* or *RSP3* (Fig. 2B). Deletion of the ORFs was confirmed by PCR (Fig. S2A, C–E). As predicted from the proteome data, LAX28::mNG localized to the axoneme of the *L. mexicana* promastigote flagellum, with some signal also in the cell body (Fig. 2B). The flagellar signal was completely lost in *ΔCFAP44* and *ΔIC140* mutants; these mutants displayed a strong fluorescent signal only in the cell body and with no signal in the flagellum. In contrast, deletion of *DRC2*, *Hydin*, *LC7*, *PF16* or *RSP3* did not alter the localization of LAX28::mNG (Fig. 2B). This is consistent with the observed loss of the LAX28 protein from the *ΔCFAP44* flagellar protein samples (Table 1). Furthermore, it showed that loss of IC140 had the same disruptive effect on LAX28 localisation as loss of CFAP44.

LAX28 is required for axonemal localization of *CFAP44* and *IC140*

We next tested whether loss of LAX28 would in turn affect CFAP44 and IC140 localisation. LAX28 was deleted in cell lines expressing either *CFAP44::mNG* or *IC140::eYFP* and the deletion was confirmed by PCR as above (Fig. S2G–I). Additionally, an addback plasmid was transfected to restore expression of LAX28 in null mutants. In the parental background, *CFAP44::mNG* and *IC140::eYFP* both localized to the axoneme (Fig. 2C,D). Following *LAX28* deletion, the fluorescent signal was lost from the flagellum. Flagellar localization was restored in the LAX28 addback cell lines (Fig. 2C,D). Interestingly, deletion of *LAX28* in *IC140::eYFP* cells resulted in a strong IC140::eYFP cell body signal. This was not observed for CFAP44::mNG in *ΔLAX28* mutants or IC140::eYFP in *ΔCFAP44* mutants. The biological significance of this is currently unclear. It is possible that this is a technical artefact. Alternatively, it may reflect differences in turnover of unassembled CFAP44 or IC140 proteins. Western blot analysis of the fluorescent fusion proteins (Fig. S3) showed that levels of the respective CFAP44::mNG or IC140::eYFP reporter proteins remained comparable before and after *LAX28* deletion, and following restoration of LAX28 expression (Fig. S3), indicating that the steady-state levels of CFAP44::mNG and IC140::eYFP are largely independent of LAX28.

Taken together, these results suggest an essential function for LAX28 in the correct axonemal localisation of CFAP44 and

Journal of Cell Science (2020) 133, jcs239855. doi:10.1242/jcs.239855

Table 1. Quantitative proteomics of *ΔCFAP44* mutant-derived flagellar axonemes

		Salt-extracted axonemes of *Cas9 T7* parental vs *ΔCFAP44* in this study			Flagellar proteome of *L. mexicana* promastigotes (Beneke et al., 2019)			
			SINQ spectral count		SINQ spectral count			
GeneID	Protein	Unique peptides	*Cas9 T7* parental	*ΔCFAP44*	Cell body insoluble	Cell body soluble	Flagellar insoluble	Flagellar soluble
LmxM.14.1430	CFAP44	38	47	0	5	0	77	0
LmxM.30.3150	CFAP43	31	38	0	9	0	107	0
LmxM.27.1630	IC140	3	3	0	0	0	14	0
LmxM.24.1310	LAX28	5	7	0	1	0	8	0
LmxM.32.2630	IC138	Not detected			0	0	19	0
LmxM.33.3880	DHC 1α	90	99	42	78	4	256	7
LmxM.23.1310	DHC 1β	62	75	29	85	7	238	5
LmxM.13.1650	αDHC/ODA11 (LmβDHC)	121	131	118	201	60	433	143
LmxM.25.0980	γDHC/ODA2 (LmαDHC)	121	135	132	226	45	546	108
LmxM.16.1430	PFR2	68	294	341	153	83	340	155
LmxM.28.0050	DRC2	25	20	28	4	0	28	0
LmxM.29.1810	Hydin	6	4	4	5	0	104	2
LmxM.20.1400	PF16	20	32	32	9	0	36	3
LmxM.18.1010	LC7	Not detected			4	1	9	6
LmxM.27.0520	RSP3	17	19	22	3	1	27	1
LmxM.24.0840	p28	5	5	4	5	0	14	0

See Table S2 for complete dataset.

IC140. Transmission electron microscopy (TEM) was used to compare the ultrastructure of *ΔLAX28* axonemes with flagella of parental cells. Multiple cross-sections of the extracellular part of the promastigote flagellum were imaged and subjected to rotational averaging (Gadelha et al., 2006; Wheeler et al., 2015). This revealed a clear lack of electron density associated with IDAs (Fig. 3A,B), supporting the conclusion that loss of *LAX28* compromises IDA structures within the flagellar axoneme.

This raised the question of whether LAX28 is required for assembly of T/TH and IDA proteins into the axoneme, or whether the absence of LAX28 renders these structures instable following assembly. *Leishmania*, like trypanosomes, offer the opportunity to examine flagella that are being actively assembled in a cell alongside its old flagellum (Wheeler et al., 2011). The localization of LAX28::mNG, CFAP44::mNG or IC140::eYFP was imaged at different points in the cell cycle, at the end of G_1 or the beginning of S phase [i.e. cells with 1 kinetoplast (K), 1 nucleus (N) and 1 flagellum (F)], at the beginning of new flagellum growth (1K 1N 2F) and following initiation of cytokinesis (2K 2N 2F) (Fig. 4; Fig. S4). In the parental background, these three fusion proteins all showed a strong fluorescence signal uniformly distributed along the axonemes of old flagella and growing new flagella. Deletion of *LAX28* in CFAP44::mNG- or IC140::eYFP-expressing cells resulted in loss of the fusion protein from old and new flagella equally (Fig. 4). If loss of LAX28 merely rendered the T/TH and IDA structures less stable post assembly, one might expect to find a stronger fluorescence signal in a growing new flagellum compared to an old one. The fact that this was not the case suggests that loss of LAX28 prevented stable incorporation of these proteins into the axoneme. The same results were obtained when CFAP44 or IC140 was deleted in cells expressing LAX28::mNG (Fig. S4); neither the growing nor the old flagella showed any LAX28::mNG signal. These data indicate that *Leishmania* CFAP44, IC140 and LAX28 are mutually dependent for their assembly into the axoneme.

ΔLAX28, *ΔCFAP44*, *ΔCFAP43* and *ΔIC140* mutants have slower swimming speeds and reduced directionality

Based on the protein localisation patterns and dependencies described above, *ΔCFAP44*, *ΔIC140* and *ΔLAX28* mutants would be expected to exhibit similar phenotypes linked to impaired IDA f function. To test this, their respective swimming speeds and velocities were measured, and the proportion of flagellar curls within the cell populations counted, comparing the characterised *ΔCFAP44*, *ΔCFAP43* and *ΔIC140* lines (Beneke et al., 2019), and newly generated *ΔLAX28* (Fig. S5) and addback cell lines. All four deletion mutants showed higher flagellar curling rates compared to the parental cell line and *ΔLAX28* addback cells (Fig. 5A). The swimming speed for *ΔLAX28* was 3.8±0.3 µm/s; for *ΔCFAP44* 2.9±0.03 µm/s; for *ΔCFAP43* 3.3 ±0.2 µm/s and for *ΔIC140* 2.9±0.2 µm/s (mean±s.d., Fig. 5B,C). By contrast *ΔLAX28* addback cells showed swimming behaviours that were similar to parental cells (Fig. 5B,C). In a plot of swimming speed versus directionality, these mutants clustered closely together, showing reduced swimming speed and directionality compared to that in the parental controls. However, their reduction in swimming speed was not as severe as that observed in *ΔPF16* and *ΔHydin* mutants [*ΔPF16* 2.0±0.1 µm/s; *ΔHydin* 2.6±0.2 µm/s, mean±s.d. (Beneke et al., 2019)] and the IDA and T/TH mutants showed more directionality compared to the uncoordinated *ΔMBO2* mutants (Beneke et al., 2019) (Fig. 5B). Flagellar lengths of Δ*LAX28*, Δ*CFAP44* and Δ*IC140* were found to be similar. Although the average lengths were slightly reduced compared to the parental control, a Student's *t*-test showed that these were not significant differences [*ΔLAX28* 15.59±3.16 µm (*P* value 0.15), *ΔCFAP44* 15.31±3.92 µm (*P* value 0.099), *ΔIC140* 15.78±3.74 µm (*P* value 0.27), Cas9 T7 parental 16.62±3.91 µm; mean±s.d., *n*=50]. Thus, the IDA f and T/TH mutants retained residual capacity for generation of a flagellar beat that results in displacement of cells, albeit at reduced speed.

LAX28 shows similarity to the human testis-expressed protein 47

While LAX28 is clearly conserved across kinetoplastids, we noted a relatively low sequence identity of only 31% between the syntenic

Journal of Cell Science (2020) 133, jcs239855. doi:10.1242/jcs.239855

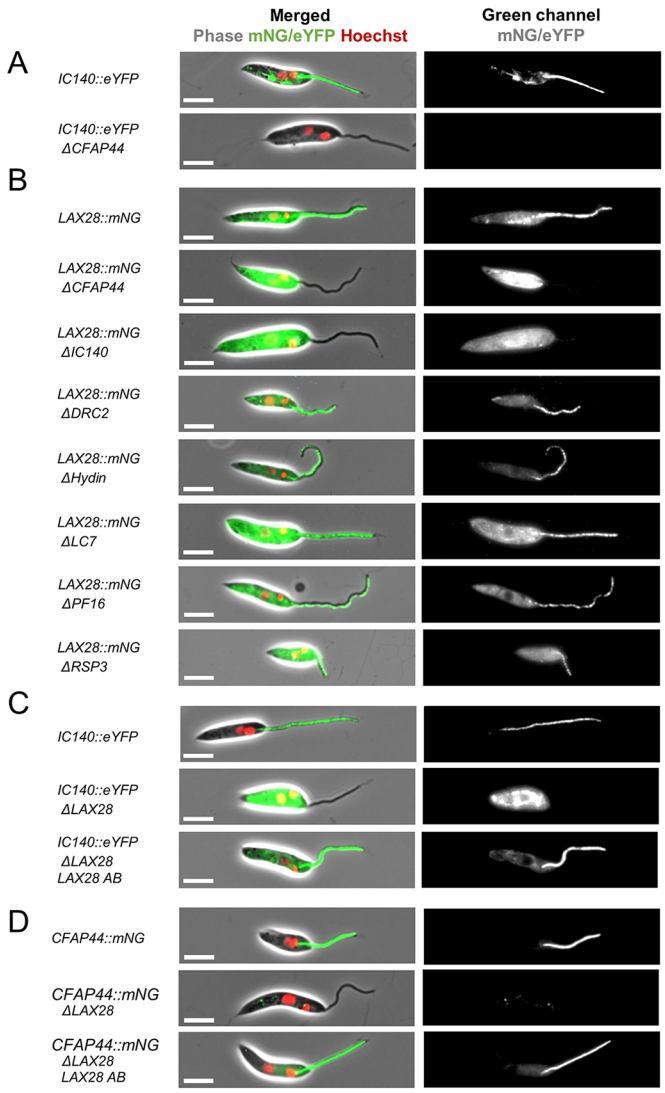

Fig. 2. IC140 and CFAP44 are required for flagellar localization of LAX28. Fluorescence micrographs showing the following *L. mexicana* cell lines: (A) *L. mexicana IC140::eYFP* and *L. mexicana IC140::eYFP ΔCFAP44*; (B) *L. mexicana LAX28::mNG* and seven different gene deletion lines, as indicated, in the *L. mexicana LAX28::mNG* background; (C) *L. mexicana IC140::eYFP, L. mexicana IC140::eYFP ΔLAX28*, and the addback cell line *L. mexicana IC140::eYFP ΔLAX28 pTadd-LAX28* (*LAX28* AB); (D) *L. mexicana CFAP44::mNG, L. mexicana CFAP44::mNG ΔLAX28*, and the addback cell line *L. mexicana CFAP44::mNG ΔLAX28 pTadd-LAX28* (*LAX28* AB). Left column, merged phase and fluorescence channels (red, Hoechst 33342-stained DNA, green, mNG or eYFP signal, respectively). Right column, greyscale rendition of green fluorescence channel. Scale bars: 5 µm.

orthologues from *L. mexicana* (LmxM.24.310) and *T. brucei* (Tb927.8.6920), and initial simple protein BLAST searches did not identify any homologues outside of this lineage. A Position-Specific Iterated BLAST (PSI BLAST; Altschul et al., 1997) search identified the uncharacterized 29.5 kDa human testis-expressed protein 47 (UniProt Q8TBZ9, TEX47/C7orf62) as a possible homologue (E value 1×10^{-60}, 16.7% sequence identity), together with uncharacterised proteins from a range of eukaryotic taxa, many annotated as C7orf62 homologues or TEX47-like. The PSI BLAST search also identified a 26 kDa *Chlamydomonas* protein CHLRE_01g038750v5 (E value 2×10^{-47}, 15.4% sequence identity). Interestingly, this is MOT7, which has been reported to

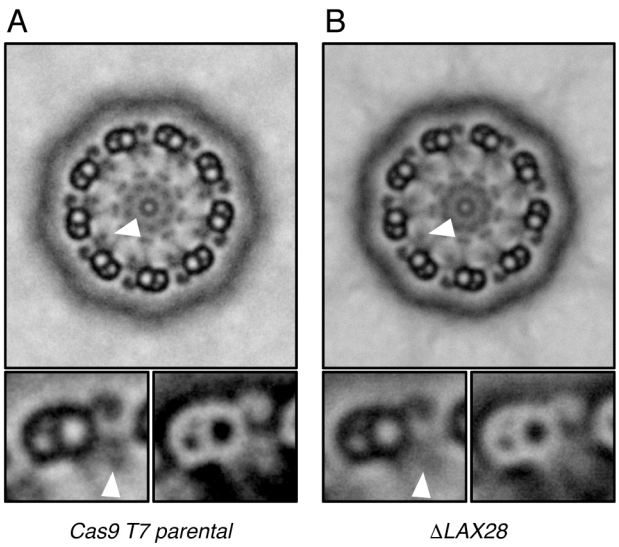

Fig. 3. Loss of LAX28 affects IDA structure. Rotational averages of transmission electron micrographs. Nine rotational averages are stack-averaged for each (A) *L. mexicana Cas9 T7* parental cells and (B) *ΔLAX28* mutants. Arrows point to the position of the IDA.

interact with T/TH complex proteins (Kubo et al., 2018). LAX28, TEX47 and MOT7 are all of a similar size, yet the primary sequence similarity is low (Fig. 6A). Nevertheless, Phyre[2] modelling (Kelley et al., 2015) predicted that all three are able to adopt very similar 3D folds, as found in flavin adenine dinucleotide (FAD)-binding protein domains of the 'sensors of blue-light using FAD' (BLUF) family (Gomelsky and Klug, 2002) (Fig. 6B).

Taken together, these results show that LAX28 is essential for normal flagellar motility and indicate that the reduced flagellar motility in *ΔLAX28* cells is linked to IDA f deficiency. Sequence comparisons suggest that MOT7, and TEX47 may be homologues of LAX28, possibly aiding motility of *Chlamydomonas* and human sperm, respectively.

DISCUSSION

LAX28 is an IDA component required for assembly of IDA f

The aim of this study was to identify proteins that interact with the T/TH complex in *Leishmania*. By comparing flagellar skeleton preparations of the *ΔCFAP44* mutants and control cells, LAX28 was identified as a new potential interactor of the IDA f–T/TH complex. Localisation of fluorescent fusion proteins in mutant and control cells showed clearly that LAX28 is an axonemal protein, and that its localization was dependent on the presence of CFAP44 and IC140. Interestingly, this dependency was found to be reciprocal, as both CFAP44 and IC140 were lost from the axoneme in *ΔLAX28* mutants. One likely explanation for these observations is that LAX28 is required for incorporation of the IDA f and the T/TH complex into the 96 nm repeat. This would also explain the loss of IDA electron density observed by TEM.

Tracking *in situ* tagged IC140 and CFAP44 proteins in *ΔLAX28* mutants through the cell cycle provided supporting evidence for a role of LAX28 in IDA f assembly. In *Chlamydomonas*, IC140 binds directly to both microtubules and plays a critical role in assembly, axonemal targeting and regulation of dynein complex f (Hendrickson et al., 2013). IC140 has been shown to be required for assembly of both heavy chains (DHC 1α, DHC 1β) and the IDA f ICLC complex (Perrone et al., 1998; Viswanadha et al., 2014). IC140 and both heavy chains form a 20S complex and preassemble

Journal of Cell Science (2020) 133, jcs239855. doi:10.1242/jcs.239855

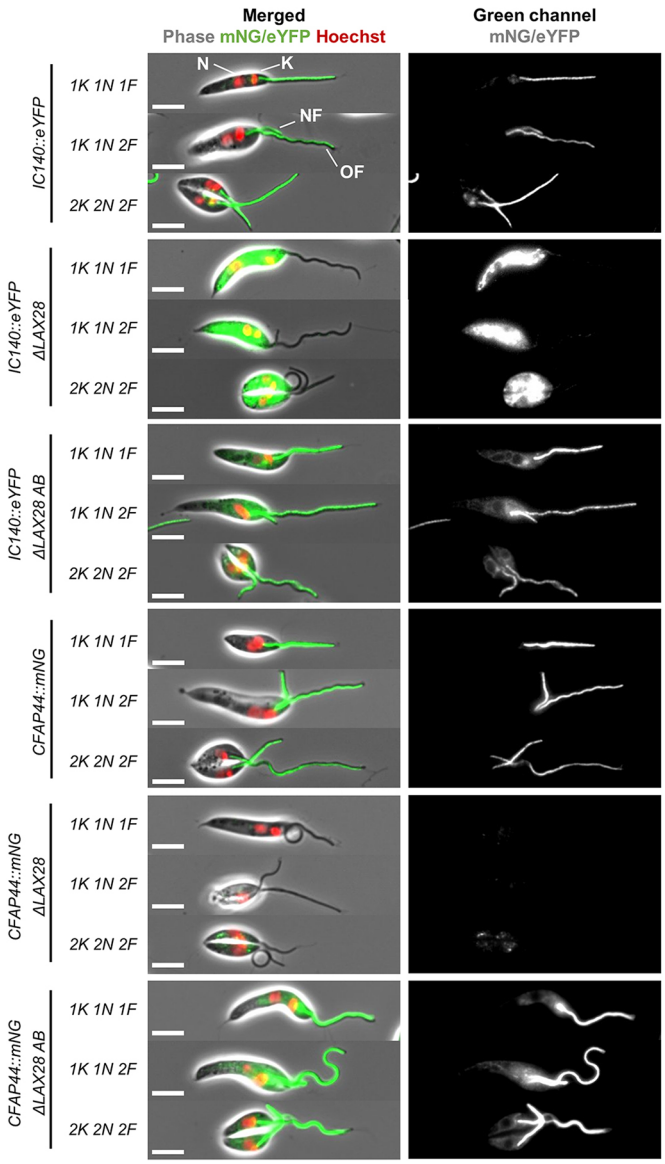

Fig. 4. LAX28 is required for flagellar localization of IC140 and CFAP44. Fluorescence micrographs showing *L. mexicana* cell lines expressing IC140::eYFP or CFAP44::mNG reporter proteins, cell lines expressing these reporter proteins and carrying a *ΔLAX28* deletion, and deletion cell lines expressing an addback (AB) copy of LAX28, as indicated on the left. Three different cell cycle stages are shown for each cell line, staged according to the number of kinetoplasts (K), nuclei (N) and Flagella (F). Left column: merged phase and fluorescence channels; red, Hoechst 33342-stained DNA, green, mNG or eYFP signal, respectively. Right column: greyscale rendition of green fluorescence channel. Scale bars: 5 µm.

in the cytoplasm before being transported by IFT proteins to the distal end of a growing flagellum (Viswanadha et al., 2014). If a similar mechanism operates in *Leishmania*, the strong cell body signal in *IC140::eYFP* cells in the absence of *LAX28* (Fig. 2C) may show the preassembled IDA f complex, which then cannot be incorporated at the tip of the growing flagellum. The observed LAX28::mNG accumulation in the cell body of *ΔIC140* or *ΔCFAP44* mutants may have a similar explanation (Fig. 2B). This is in contrast to the complete loss of CFAP44::mNG signal following loss of *LAX28* (Fig. 2D) and complete depletion of IC140::eYFP signal in *ΔCFAP44* mutants (Fig. 2A). Setting aside the possibility of technical variations, this could indicate that CFAP44 is not assembled into the IDA f 20S complex in the cytoplasm or is subject to more rapid turnover in cells that lack LAX28, and that IC140 is degraded more quickly in absence of CFAP44.

Loss of LAX28 reduces swimming speed and directionality to levels similar to those observed for *ΔIC140* or *ΔCFAP44* mutants, consistent with a functional link between these proteins in *Leishmania.* With respect to flagellar curling rates, the *ΔLAX28* cells (38% curling) do, however, not fully phenocopy the *ΔIC140* cells (67% curling). There are at least two alternative explanations that could account for this discrepancy. First, that the loss of LAX28 reduced IC140 protein to levels below the detection limit of the fluorescence microscope, but it is possible that a sufficiently small number of IC140 proteins remained in the axoneme, so that curling rates in *ΔLAX28* mutants remained below those observed in an *IC140* null mutant. Alternatively, the loss of LAX28 may affect other IDA-related structures in addition to IDA f, either some of the single-headed IDAs or accessory complexes. This loss may counteract the effect of IC140 loss to some extent, so that the net result is an intermediate rate of curling.

While the reduction of TEM electron density at the location of IDAs in *ΔLAX28* mutants (Fig. 3) is consistent with an IDA f assembly defect, the residual electron density indicates that at least some of the other IDA heavy chains (a–e and g) remain. This aligns with previous findings in *Chlamydomonas*, where each IDA is independently targeted to its location within the 96 nm repeat, causing gaps if assembly of one IDA fails. This gap will be reflected as reduced electron density in thin sections, but not complete absence of signal (Bui et al., 2012; Heuser et al., 2012; Piperno, 1990). In *Leishmania*, the flagella of IDA f deletion mutants are not completely paralysed but their swimming speed and directionality is reduced compared to that found in wild-type cells (Beneke et al., 2019) (Fig. 5B,C). Similar observations have been made for *ΔIC140* mutants and IDA f–T/TH complex mutants in *Chlamydomonas*. *ΔFAP44* and *ΔIC140* mutants showed only moderate flagellar beat and swimming defects compared to other ODA- or IDA-heavy chain deficient mutants, which are more severe (Kato-Minoura et al., 1997; Kubo et al., 2018; Perrone et al., 1998). While it is clear that LAX28 is required for normal motility and function of the *Leishmania* flagellum, defining the precise IDA assembly defects and fate of the other IDA heavy chains (a–e and g) and other ultrastructural changes will require cryo-electron microscopy (cryo-EM) reconstructions of parental and *ΔLAX28* mutant axonemes.

The IDA f and T/TH complex shows diversity across flagellated eukaryotes

Biochemical studies and cryo-EM reconstructions of the *Chlamydomonas* T/TH complex showed FAP44 to be a constituent of the tether, and demonstrated direct interactions between FAP44, FAP43 and IDA f dynein motor domains I1α and I1β (Fu et al., 2018; Kubo et al., 2018). The tether is anchored to the axoneme through the C-terminal coiled-coil domains of FAP44 and FAP43. Ultrastructural comparisons between wild-type and *fap44* mutants suggested that the tether constrains the nucleotide-dependent movement of the IDA f head domains (Kubo et al., 2018) and indicated a role for FAP44 in the assembly of the IDA f dynein motor but not the ICLC (Fu et al., 2018). This is in contrast to the results from *L. mexicana*, where mass spectrometry data from salt-extracted flagellar preparations and *in situ* tagging showed a loss of IC140 in *ΔCFAP44* mutants as well as a reduction of both IDA I1 α and β heavy chains (Table 1, Fig. 2A). *L. mexicana* CFAP43 was also lost from *ΔCFAP44* mutant axonemes, in line

Journal of Cell Science (2020) 133, jcs239855. doi:10.1242/jcs.239855

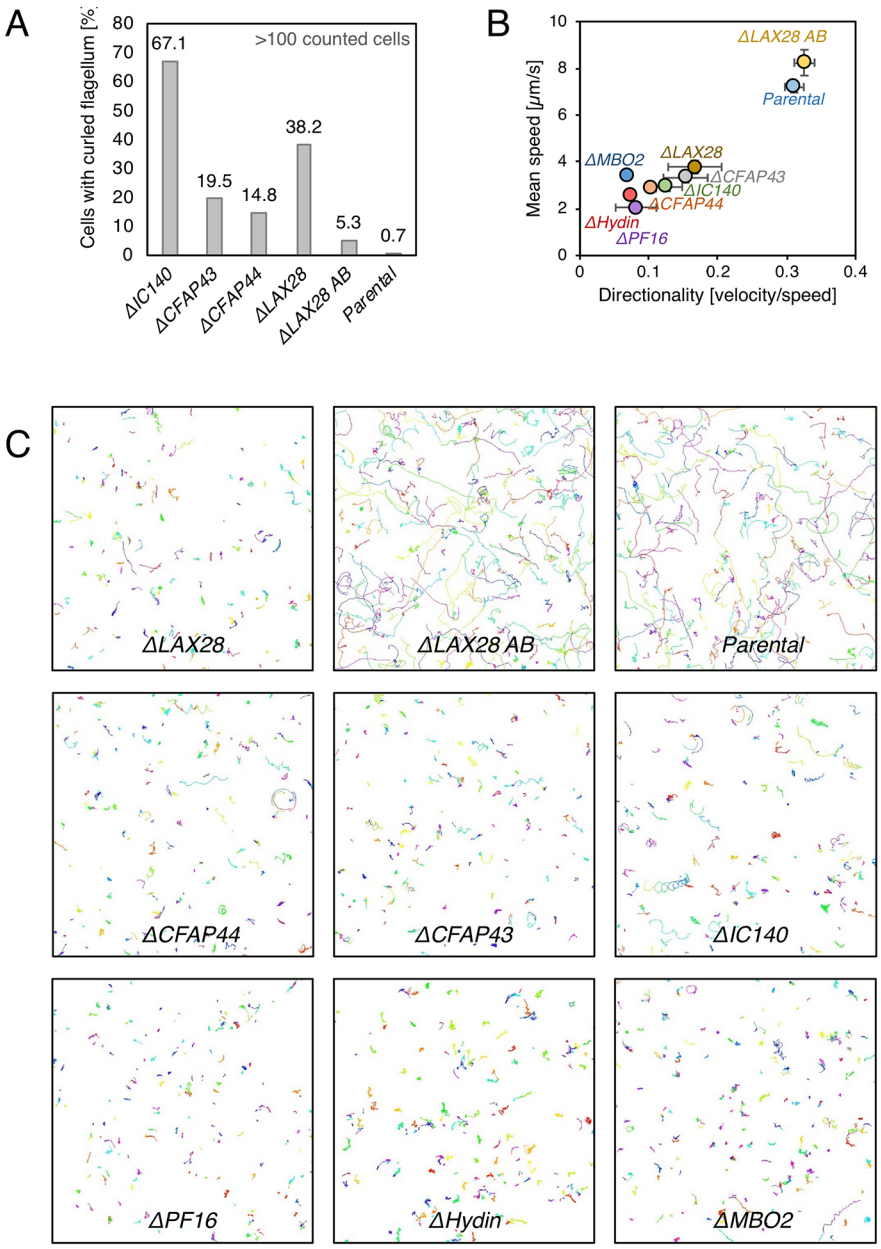

Fig. 5. LAX28 is essential for normal flagellar motility. (A) Histogram showing the proportion of cells with curled flagella in *ΔIC140* (*n*=184), *ΔCFAP43* (*n*=118), *ΔCFAP44* (*n*=210) and *ΔLAX28* (*n*=141) mutants, the parental *L. mexicana Cas9 T7* cell line (*n*=296) and *ΔLAX28* expressing a LAX28 addback copy (AB; *n*=143). Numbers above the bars indicate percentage of cells with curly flagella. (B) Plot showing mean swimming speed and directionality (the ratio of velocity to speed) for the indicated cell lines. Each point represents the average of three measurements, each replicate representing a separate slide prepared from one culture. Error bars represent the standard deviation of the three replicates. (C) Swimming paths used for extracting mean swimming speed and directionality shown in B; 200 paths are shown for each cell line.

with the finding that the *Chlamydomonas* T/TH complex requires dimerization of CFAP43/FAP43 and CFAP44/FAP44 for it to be assembled (Fu et al., 2018; Urbanska et al., 2018). Furthermore, our data show that *L. mexicana* CFAP44 and IC140 are both dependent on LAX28. These data suggest the *Leishmania* T/TH complex cannot assemble in the absence of the IDA f complex, contrary to the case in *Chlamydomonas* (Heuser et al., 2012; Fu et al., 2018). Further, more detailed, studies of the *L. mexicana* wild-type axoneme ultrastructure could help to define the precise location of LAX28 relative to the T/TH and IDA f complex and define the fate of the T/TH structure in a range of defined IDA f mutants.

Of the known T/TH-associated proteins, CFAP44, CFAP43 and Fap57p (Urbanska et al., 2018) seem to be well conserved across flagellated eukaryotes, including *Trypanosoma*. Fap57p has been identified to be a homologue of CMF6 and CMF5 in *T. brucei* (Baron et al., 2007). A partial *L. mexicana CMF6* deletion mutant showed swimming patterns similar to *ΔLAX28*, *ΔCFAP44* and *ΔIC140* knockouts (Beneke et al., 2019). Other T/TH-associated proteins reported to date appear to be rather restricted to the taxa in which they were found; *Chlamydomonas* proteins Cre10.g452250 (Kubo et al., 2018) and FAP244 were identified to be part of the T/TH complex but have no homologue in *Tetrahymena* and other organisms (Fu et al., 2018). Interestingly, CFAP44, CFAP43, Fap57p and FAP244 all share similar domain architectures, with N-terminal WD40 repeats and C-terminal coiled-coil domains (Fu et al., 2018; Urbanska et al., 2018), and FAP43 and FAP244 can functionally compensate for each other (Kubo et al., 2018).

We showed here that MOT7 (Kubo et al., 2018) shares some similarities with LAX28, as well as TEX47, but the sequence identity is too low to conclude homology with confidence. LAX28, TEX47 and MOT7 do not show clear signatures of known domains but may be able to adopt a similar three-dimensional fold, as Phyre[2] modelling predicted a β-sheet with four or five strands and two or three α helices for all three proteins, revealing similarities to FAD-binding domains of the BLUF family. BLUF domains were first identified in *Euglena* (Iseki et al., 2002) and bacteria (Masuda and

Journal of Cell Science (2020) 133, jcs239855. doi:10.1242/jcs.239855

A

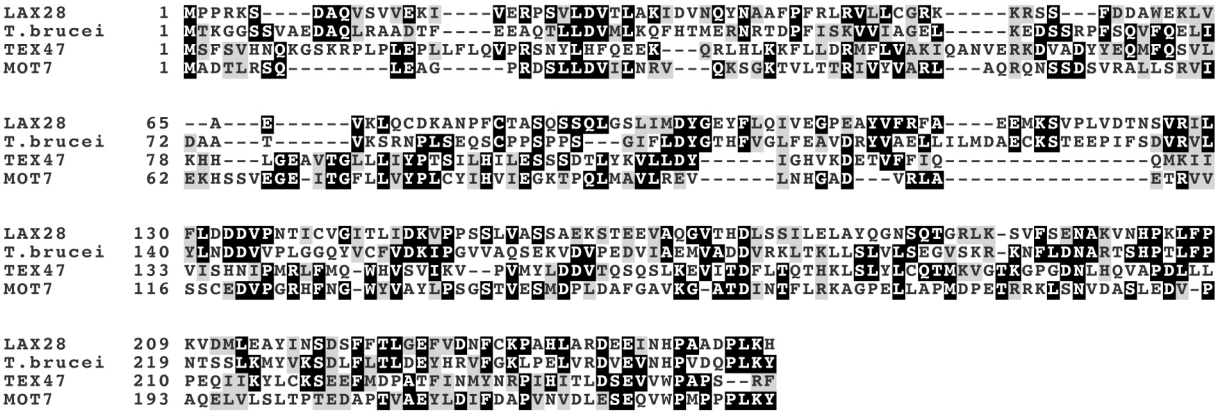

B

Template ID		Query sequence (% confidence / rank)		
		LAX28	TEX47	MOT7
c2hfnJ	Molecule: synechocystis photoreceptor	96.7 / 1	98.6 / 1	98.2 / 3
d1x0pa1	Fold: Ferredoxin-like; Superfamily: Acylphosphatase/BLUF domain-like	96.6 / 2	98.5 / 2	98.3 / 1
d1yrxa1	Fold: Ferredoxin-like; Superfamily: Acylphosphatase/BLUF domain-like	96.6 / 3	98.3 / 6	98.3 / 2

Fig. 6. Similarity between LAX28 and human TEX47. (A) Multiple sequence alignment (Sievers et al., 2011) of LAX28 (XP_003875945/LmxM.24.1310) with the syntenic orthologue from *T. brucei* (XP_847522 conserved hypothetical protein/Tb927.8.6920) and putative homologues from *H. sapiens* (NP_689919.1 testis-expressed protein 47; TEX47) and *C. reinhardtii* (PNW88650.1 hypothetical protein CHLRE_01g038750v5; MOT7), identified by a PSI-BLAST search of the non-redundant protein sequences (nr) in the NCBI database (using default parameters and three iterations). Shading was applied using Boxshade (https://embnet.vital-it.ch/software/BOX_form.html) where the fraction of matching sequences is at least 0.5, with black indicating identity and grey similarity. (B) Results of remote homology detection and 3D fold prediction by Phyre^2 (Kelley et al., 2015). Searches with LAX28, TEX47 or MOT7 all identified good matches with BLUF domain proteins, returning an overlapping set of highest-ranking hits, with high confidence scores of >96%.

Bauer, 2002) and have been linked to sensing blue light (Gomelsky and Klug, 2002). Interestingly, the blue-light-sensing protein identified in *Euglena gracilis* has been characterised as a photoactivated adenylyl cyclase containing two BLUF domains, and has been shown to regulate flagellar motility by controlling intraflagellar levels of cyclic AMP (Iseki et al., 2002). A role in light-sensing for MOT7 seems worth exploring, since *Chlamydomonas* clearly undergoes phototaxis (Bennett and Golestanian, 2015). While *Leishmania* is not known to respond to light, BLUF domains may also function in redox-dependent signal transduction (Gomelsky and Klug, 2002). Thus, whether LAX28 is required only for IDA assembly or whether it contributes more directly to its regulatory role in the axoneme remains to be studied.

Given the role of IDA f as a regulatory hub for the modulation of flagellar waveforms one might perhaps predict that this is precisely where cell-type or species-specific proteins are required. Their role might be to orchestrate the conserved basic mechanisms of flagellar bend generation in biologically appropriate ways to produce the observed diversity of beating patterns. Further work in this area will no doubt benefit from comparative studies between cell types with a range of different behaviours.

While the precise phylogenetic relationship, if any, between LAX28, TEX47 and MOT7 remains to be established, TEX47 should be followed up for a possible link to male infertility. Male infertility affects ∼7% of men and the genetic cause for this disease has been identified for only 25% of cases. While more than 3000 genes have been associated with spermatogenesis, less than 0.01% of these have been linked to infertility (reviewed in Neto et al., 2016). Compound-heterozygous mutations and frameshift mutations in CFAP44 and CFAP43 have been connected to male infertility (Tang et al., 2017). While, to our knowledge, mutations in TEX47 have not yet been linked to male infertility, the predominant expression of TEX47 in human testis (Fagerberg et al., 2014), its presence in the human sperm tail proteome (Amaral et al., 2013) and the results presented in this study for LAX28 suggest it may have a role in the regulation of sperm motility.

MATERIALS AND METHODS

Cell culture

Promastigote forms of *L. mexicana Cas9 T7* (Beneke et al., 2017; derived from *L. mexicana* WHO strain MNYC/BZ/62/M379) were grown at 28°C in M199 medium (Life Technologies) supplemented with 2.2 g/l $NaHCO_3$, 0.005% haemin, 40 mM HEPES pH 7.4 and 10% fetal calf serum (FCS). 50 µg/ml nourseothricin sulphate and 32 µg/ml Hygromycin B were included before transfection with pPLOT or pT cassettes. For selection and maintenance of genetically modified *L. mexicana Cas9 T7* lines generated in this study the relevant selection drugs were added to supplemented M199 medium as described in Beneke et al. (2017).

Salt-extracted axonemes

A widely utilized isolation protocol for *T. brucei* flagellar skeletons (Robinson and Gull, 1991) was adapted for use in *L. mexicana*. Cells were first extracted with non-ionic detergent in 1% octyl glucoside to yield whole-cell cytoskeletons and then salt extracted on ice using 1 M NaCl to depolymerize subpellicular microtubules. To avoid proteolytic degradation, all procedures were performed on ice or at 4°C during centrifugations. $1×10^9$ *L. mexicana ΔCFAP44* mutants and *L. mexicana Cas9 T7* parental cells were collected at 800 ***g*** for 15 min and resuspended in 2.5 ml phosphate-buffered saline (PBS), containing a protease inhibitor cocktail [final concentration, 1× Halt Protease Inhibitor Cocktail (Thermo Fisher Scientific, containing 1 mM AEBSF-HCl, 0.8 µM aprotinin, 50 µM

bestatin, 15 µM E64, 20 µM leupeptin, 10 µM pepstatin A) supplemented with 500 µM PMSF and 5 mM EDTA]. 50 µl of cell suspension was isolated and supplemented with 5 µl 20% SDS solution (Fig. 1i). The remaining cell suspension was centrifuged again and resuspended in 2.5 ml 10 mM PIPES [10 mM NaCl, 10 mM piperazine-N,N′-bis(2-ethanesulfonic acid), 1 mM $CaCl_2$, 1 mM $MgCl_2$, 0.32 M sucrose, adjusted to pH 7.2], containing protease inhibitor cocktail and octylglucoside [1% (w/v) final concentration]. Cells were left on ice for 5 min and centrifuged for 10 min at 2000 ***g***. 50 µl of supernatant was isolated and supplemented with 5 µl 20% SDS solution (Fig. 1, s/n 1). Then, 1.25 ml cold 10 mM PIPES buffer, containing protease inhibitor cocktail, octylglucoside [1% (w/v) final concentration] and 1 M NaCl was added to the pellet and vortexed for 60 s. After incubation for 30 min on ice, the solution was centrifuged at 12,200 ***g*** for 20 min. 50 µl of supernatant was isolated and supplemented with 5 µl 20% SDS solution (Fig. 1, s/n 2). The pellet was resuspended in 1 ml cold 10 mM PIPES buffer, containing a protease inhibitor cocktail and 0.32 M sucrose. The sample was loaded on top of a sucrose bed containing one layer of 10 mM PIPES with 33% w/v sucrose [10 mM NaCl, 10 mM piperazine-N,N′-bis(2-ethanesulfonic acid), 1 mM $CaCl_2$, 1 mM $MgCl_2$, adjusted to pH 7.2 with 0.96 M sucrose] and centrifuged at 800 ***g*** for 15 min. While the top layer was centrifuged again at 12,200 ***g*** for 20 min the remaining sucrose bed was discarded. After centrifugation, the supernatant was discarded and the pellet resuspended in 100 µl PBS containing protease inhibitor cocktail and 2% SDS (Fig. 1iv). Proteins were quantified using BCA assay. For Coomassie, gel samples were mixed with 4× Laemmli buffer (1× final concentration) and heated at 60°C for 10 min. For proteomic analysis, ∼4 µg of protein (∼50 µl) of the final fraction (iv) were analysed by liquid tandem mass spectrometry.

Proteomics

Protein samples were prepared using filter-aided sample preparation (FASP) digestion (Wiśniewski et al., 2009) (Vicacon500, Sartorius, VN01H02 10 kDA). The FASP filter were washed with 200 µl 0.1% trifluoroacetic acid (TFA) in 50% acetonitrile (ACN) (14,300 ***g***, 10 min) and ∼4 µg of protein was loaded onto the filter. Samples were denatured with 200 µl 8 M urea in 100 mM triethylammonium bicarbonate (TEAB) for 30 min at room temperature, reduced with 10 mM tris(2-carboxyethyl)phosphine hydrochloride (TCEP) for 30 min at room temperature and alkylated with 50 mM chloroacetamide (CAA) for 30 min at room temperature in the dark. FASP columns were centrifuged (14,300 ***g***, 10 min) and washed first multiple times with 200 µl 6 M urea in 50 mM TEAB until no more bubbles formed and were then washed twice with 200 µl 1 M urea in 50 mM TEAB. FASP columns were centrifuged again. Samples were digested with 200 ng trypsin in 300 µl 50 mM TEAB overnight at 37°C. Columns were centrifuged and flow through was kept. Columns were washed with 200 µl 0.1% TFA and with 200 µl 50% ACN in 0.1% TFA. The flow through was collected from both washes. Samples were dried in a SpeedVac, resuspend in 50 µl 5% formic acid and 5% DMSO and then trapped on a C18 PepMap100 pre-column [300 µm internal diameter (i.d.) ×5 mm, 100 Å, Thermo Fisher Scientific] using solvent A (0.1% formic acid in water) at a pressure of 500 bar and separated on an Ultimate 3000 UHPLC system (Thermo Fisher Scientific) coupled to a QExactive mass spectrometer (Thermo Fisher Scientific). The peptides were separated on an in-house packed analytical column (360 µm×75 µm i.d. packed with ReproSil-Pur 120 C18-AQ, 1.9 µm,120 Å, Dr. Maisch, GmbH) and then electro sprayed directly into an QExactive mass spectrometer (Thermo Fisher Scientific) through an EASY-Spray nano-electrospray ion source (Thermo Fisher Scientific) using a linear gradient [length: 60 min, 15% to 38% solvent B (0.1% formic acid in ACN), flow rate, 200 nl/min]. The raw data was acquired on the mass spectrometer in a data-dependent mode (DDA). Full scan MS spectra were acquired in the Orbitrap (scan range 350–2000 *m*/*z*, resolution 70,000, AGC target 3e6, maximum injection time 50 ms). After the MS scans, the 20 most intense peaks were selected for HCD fragmentation at 30% of normalised collision energy. HCD spectra were also acquired in the Orbitrap (resolution 17,500, AGC target 5e4, maximum injection time 120 ms) with first fixed mass at 180 *m*/*z*.

Proteomic analysis

MS data were analysed as previously described (Beneke et al., 2019). Briefly, MS data were converted from .RAW to .MGF files using ProteoWizard and uploaded to the Central Proteomics Facilities Pipeline (CPFP; Trudgian et al., 2010). Protein lists were generated by using CPFP meta-searches against the predicted *L. mexicana* proteome (gene models based on Fiebig et al., 2015), followed by label-free SINQ quantification (Table S1). Proteins that were exclusively identified in *ΔCFAP44* mutants were generally of low abundance (two or three detected peptides; Tables S1 and S2), with the exception of β-tubulin (LmxM.08.1230) for which 48 detected peptides were recorded in *ΔCFAP44* mutants. However, only one out of those 48 peptides was unique (spectral count 1; Tables S1 and S2). This suggests that proteins exclusively identified in the *ΔCFAP44* mutants may represent false positives and they were not further analysed in this study. The mass spectrometry proteomics data have been deposited to the ProteomeXchange Consortium via the PRIDE (Vizcaíno et al., 2016) partner repository with the dataset identifier PXD014077.

Solubilisation experiments

Solubilisation of CFAP44 was tested using a reporter cell line, expressing *in situ* tagged *CFAP44::eYFP* fusion protein generated using the method described in Beneke and Gluenz (2019). 1×10^7 cells were collected at 800 ***g*** for 5 min and washed once in PBS. Cells were pelleted again and resuspended in 100 µl of 10 mM PIPES buffer (as above), containing a protease inhibitor cocktail (as above) and octylglucoside [1% (w/v) final concentration], as well as either 2 M LiCl, 2 M $CaCl_2$, 3.2 M KCl or 4 M NaCl. Lower concentrations were also tested including: 0.01–0.75 M NaCl, 1 M LiCl or 0.25–1.5 M $CaCl_2$. Cell suspensions were vortexed for 60 s and incubated for 30 min on ice. The solution was centrifuged at 17,000 ***g*** for 2 min and the pellet washed once in PBS. Cells were pelleted again, resuspended in 10 mM PIPES buffer and pipetted onto a glass slide for viewing under a microscope.

CRISPR-Cas9 gene knockouts and tags

Gene deletion and tagging was essentially done as described in Beneke et al. (2017). The online primer design tool www.LeishGEdit.net was used to design primers for amplification of the 5′ and 3′ sgRNA templates and for amplification of donor DNA from pT and pPLOT plasmids. Following transfection with pPLOT cassettes, limiting dilution was used to generate clonal tagged cell lines (Beneke and Gluenz, 2019). These were then subjected to gene deletions using two different pT cassettes and selected as populations.

Addback construction

The ORF of LAX28 was amplified using primers F: 5′-TTAGCAACTA-GTATGGAACAGAAGCTGATCAGCGAAGAAGACCTGGAGCAAA-AGCTCATTAGCGAGGAGGACCTCATGCCTCCGCGCAAGTCAGA-3′ and R: 5′-TTAGCACCATGGGCGCGGGTTCATTTTATCGT-3′ and cloned into pTadd (Beneke et al., 2017) using *Spe*I and *Nco*I cloning sites. 5 µg of circular plasmid was transfected as described previously (Beneke et al., 2017) to allow episomal expression of *2xMyc::LAX28*. Drug-resistant cells were selected using 25 µg/ml phleomycin.

Diagnostic PCR for knockout verification

Extracted genomic DNA of drug-selected populations was subjected to diagnostic PCRs to test for the presence of the target gene ORF in putative knockout lines and the parental cell line as described previously (Beneke and Gluenz, 2019; Beneke et al., 2017) and using primer sequences reported in Beneke et al. (2019). To show the presence of genomic DNA in the test samples, a second PCR reaction was performed using primers F: 5′-CGCAGAAGGAGAAGAGCGAG-3′ and R: 5′-GTTGTACACGGACA-GCTCCA-3′ to amplify the ORF of PFR2.

Light and electron microscopy

L. mexicana expressing fluorescent fusion proteins were prepared for DNA staining with Hoechst 33342 and imaging as described previously (Wheeler et al., 2015) and immediately imaged live, with a Zeiss Axioimager.Z2 microscope with a 63× numerical aperture (NA) 1.40 oil immersion

objective and a Hamamatsu ORCA-Flash4.0 camera at the ambient temperature of 25–28°C. Micrographs were taken with a 3000 ms exposure time for the green fluorescent channel. For each cell line, at least three fields of view, each containing at least 30 cells, were captured.

For TEM, cells were prepared with a chemical fixation protocol similar to in Hoog et al. (2010). Briefly, cells were fixed with 2.5% glutaraldehyde and 4% paraformaldehyde in M199 culture medium for 2 h at room temperature. Fixed cells were washed six times for 10 min in 0.1 M PIPES buffer at pH 7.2. Wash four of six was supplemented with 50 mM glycine. Cells were embedded in 4% low-melting-point agarose and incubated in 1% osmium tetroxide and 1.5% potassium ferrocyanide in 0.1 M PIPES buffer at 4°C for 1 h in darkness. Samples were then washed five times with ddH_2O for 5 min each time and stained with 0.5% uranyl acetate in darkness at 4°C overnight. Samples were dehydrated, embedded in epoxy resin, sectioned and on-section stained as described previously (Hoog et al., 2010). Electron micrographs were captured on a Tecnai 12 TEM (FEI) with an Ultrascan 1000 CCD camera (Gatan).

Image processing

All micrographs were processed using Fiji (Schindelin et al., 2012). To allow comparison between the fluorescence signals in tagged cell lines, the same settings were used to display the green fluorescence channel. Channel settings were set for CFAP44::mNG-tagged cell lines to 7000–20,000, for IC140::eYFP-tagged cell lines at 6000–11,000 (except in Fig. 2A, 17,000 to 22,000) and for LAX28::mNG-tagged cell lines at 5000–12,000. Settings were identical for the tagged cell line and additional knockouts and addbacks on top of the tagged cell lines.

For average rotation of axonemes in TEM images, nine sections from each cell line were average rotated as previously described (Gadelha et al., 2006; Wheeler et al., 2015). The resulting images were aligned using the 'Align image by line ROI' function in Fiji (Schindelin et al., 2012). A stack was generated from these aligned images and signals were averaged by using the 'Z projection' function.

Motility analysis

Motility analysis was performed as previously described in Beneke et al. (2019) using the method from Wheeler (2017). Directionality (velocity/speed) and mean speed was measured for each mutant from three samples taken from cell cultures at a density of ∼6×10^6 cells/ml. 5 µl of cell culture was placed on a glass slide in a 250-µm deep chamber covered with a #1.5 cover slip and imaged using darkfield illumination with a 10× NA 0.3 objective and a Hamamatsu ORCA-Flash4.0 camera on a Zeiss Axioimager.Z2 microscope at the ambient temperature of 25–28°C.

Illumina sequencing

Leishmania genomic DNA was prepared using the Illumina TruSeq Nano DNA Library kit according to the manufacturer's instructions. The final sequencing pool was quantified by qPCR using the NEB Library Quant Kit and library size was determined using the Agilent High Sensitivity DNA Kit on a 2100 Bioanalyzer instrument. The final library was multiplexed with other sequencing samples and the Illumina sequencer was loaded with 1.8 pM. Sequencing was performed using a NextSeq 500/550 High Output Kit v2.5 (2×75 cycles, 6 and 8 cycles index read).

NextSeq raw files were de-multiplexed using bcl2fastq (Illumina) with 0 nt mismatch for indexes and assembled using the Burrows-Wheeler Aligner (Li and Durbin, 2009). Samtools (Li et al., 2009) was used for sorting and indexing bam files. Bam files were viewed using the IGV genome browser (Robinson et al., 2011).

Acknowledgements

We would like to thank Svenja Hester and Philip Charles (Central Proteomics Facility) for help with protein mass spectrometry, Errin Johnson and Raman Dhaliwal (Dunn School Bioimaging Facility) for assistance with electron microscopy and Keith Gull (University of Oxford) for sharing equipment funded by the Wellcome Trust.

Competing interests

The authors declare no competing or financial interests.

Author contributions

Conceptualization: T.B., E.G.; Methodology: T.B., E.G.; Formal analysis: T.B., K.B., S.F.; Investigation: T.B., K.B., S.F.; Resources: E.G.; Data curation: T.B., E.G.; Writing - original draft: T.B.; Writing - review & editing: T.B., E.G.; Visualization: T.B.; Supervision: T.B., E.G.; Project administration: E.G.; Funding acquisition: E.G.

Funding statement

E.G. was supported by a Royal Society University Research Fellowship (UF100435 and UF160661). This work was supported by PhD studentships to T.B. (Medical Research Council reference 15/16_MSD_836338) and S.F. (Royal Society reference RGF\EA\180189), and Wellcome Trust grant 104627/Z/14/Z to Keith Gull (University of Oxford, UK). The funders had no role in study design, data collection and analysis, decision to publish or preparation of the manuscript.

Data availability

The mass spectrometry proteomics data have been deposited to the ProteomeXchange Consortium via the PRIDE partner repository with the dataset identifier PXD014077.

Supplementary information

Supplementary information available online at
http://jcs.biologists.org/lookup/doi/10.1242/jcs.239855.supplemental

Peer review history

The peer review history is available online at
https://jcs.biologists.org/lookup/doi/10.1242/jcs.239855.reviewer-comments.pdf

References

Adams, G. M., Huang, B., Piperno, G. and Luck, D. J. (1981). Central-pair microtubular complex of Chlamydomonas flagella: polypeptide composition as revealed by analysis of mutants. *J. Cell Biol.* **91**, 69-76. doi:10.1083/jcb.91.1.69

Altschul, S. F., Madden, T. L., Schaffer, A. A., Zhang, J., Zhang, Z., Miller, W. and Lipman, D. J. (1997). Gapped BLAST and PSI-BLAST: a new generation of protein database search programs. *Nucleic Acids Res.* **25**, 3389-3402. doi:10.1093/nar/25.17.3389

Amaral, A., Castillo, J., Estanyol, J. M., Ballescà, J. L., Ramalho-Santos, J. and Oliva, R. (2013). Human sperm tail proteome suggests new endogenous metabolic pathways. *Mol. Cell. Proteomics* **12**, 330-342. doi:10.1074/mcp.M112.020552

Barber, C. F., Heuser, T., Carbajal-González, B. I., Botchkarev, V. V., Jr and Nicastro, D. (2012). Three-dimensional structure of the radial spokes reveals heterogeneity and interactions with dyneins in Chlamydomonas flagella. *Mol. Biol. Cell* **23**, 111-120. doi:10.1091/mbc.e11-08-0692

Baron, D. M., Ralston, K. S., Kabututu, Z. P. and Hill, K. L. (2007). Functional genomics in Trypanosoma brucei identifies evolutionarily conserved components of motile flagella. *J. Cell Sci.* **120**, 478-491. doi:10.1242/jcs.03352

Beneke, T. and Gluenz, E. (2019). LeishGEdit: a method for rapid gene knockout and tagging using CRISPR-Cas9. *Methods Mol. Biol.* **1971**, 189-210. doi:10.1007/978-1-4939-9210-2_9

Beneke, T., Madden, R., Makin, L., Valli, J., Sunter, J. and Gluenz, E. (2017). A CRISPR Cas9 high-throughput genome editing toolkit for kinetoplastids. *R. Soc. Open Sci.* **4**, 170095. doi:10.1098/rsos.170095

Beneke, T., Demay, F., Hookway, E., Ashman, N., Jeffery, H., Smith, J., Valli, J., Becvar, T., Myskova, J., Lestinova, T. et al. (2019). Genetic dissection of a Leishmania flagellar proteome demonstrates requirement for directional motility in sand fly infections. *PLoS Pathog.* **15**, e1007828. doi:10.1371/journal.ppat.1007828

Bennett, R. R. and Golestanian, R. (2015). A steering mechanism for phototaxis in Chlamydomonas. *J. R. Soc. Interface* **12**, 20141164. doi:10.1098/rsif.2014.1164

Bui, K. H., Yagi, T., Yamamoto, R., Kamiya, R. and Ishikawa, T. (2012). Polarity and asymmetry in the arrangement of dynein and related structures in the Chlamydomonas axoneme. *J. Cell Biol.* **198**, 913-925. doi:10.1083/jcb.201201120

Coutton, C., Vargas, A. S., Amiri-Yekta, A., Kherraf, Z. E., Ben Mustapha, S. F., Le Tanno, P., Wambergue-Legrand, C., Karaouzène, T., Martinez, G., Crouzy, S. et al. (2018). Mutations in CFAP43 and CFAP44 cause male infertility and flagellum defects in Trypanosoma and human. *Nat. Commun.* **9**, 686. doi:10.1038/s41467-017-02792-7

Curry, A. M., Williams, B. D. and Rosenbaum, J. L. (1992). Sequence analysis reveals homology between two proteins of the flagellar radial spoke. *Mol. Cell. Biol.* **12**, 3967-3977. doi:10.1128/MCB.12.9.3967

Dawe, H. R., Shaw, M. K., Farr, H. and Gull, K. (2007). The hydrocephalus inducing gene product, Hydin, positions axonemal central pair microtubules. *BMC Biol.* **5**, 33. doi:10.1186/1741-7007-5-33

DiBella, L. M., Sakato, M., Patel-King, R. S., Pazour, G. J. and King, S. M. (2004a). The LC7 light chains of Chlamydomonas flagellar dyneins interact with

components required for both motor assembly and regulation. *Mol. Biol. Cell* **15**, 4633-4646. doi:10.1091/mbc.e04-06-0461

DiBella, L. M., Smith, E. F., Patel-King, R. S., Wakabayashi, K. and King, S. M. (2004b). A novel Tctex2-related light chain is required for stability of inner dynein arm I1 and motor function in the Chlamydomonas flagellum. *J. Biol. Chem.* **279**, 21666-21676. doi:10.1074/jbc.M313540200

Diener, D. R., Ang, L. H. and Rosenbaum, J. L. (1993). Assembly of flagellar radial spoke proteins in Chlamydomonas: identification of the axoneme binding domain of radial spoke protein 3. *J. Cell Biol.* **123**, 183-190. doi:10.1083/jcb.123.1.183

Dutcher, S. K., Huang, B. and Luck, D. J. (1984). Genetic dissection of the central pair microtubules of the flagella of Chlamydomonas reinhardtii. *J. Cell Biol.* **98**, 229-236. doi:10.1083/jcb.98.1.229

Dymek, E. E., Heuser, T., Nicastro, D. and Smith, E. F. (2011). The CSC is required for complete radial spoke assembly and wild-type ciliary motility. *Mol. Biol. Cell* **22**, 2520-2531. doi:10.1091/mbc.e11-03-0271

Fagerberg, L., Hallström, B. M., Oksvold, P., Kampf, C., Djureinovic, D., Odeberg, J., Habuka, M., Tahmasebpoor, S., Danielsson, A., Edlund, K. et al. (2014). Analysis of the human tissue-specific expression by genome-wide integration of transcriptomics and antibody-based proteomics. *Mol. Cell. Proteomics* **13**, 397-406. doi:10.1074/mcp.M113.035600

Fiebig, M., Kelly, S. and Gluenz, E. (2015). Comparative life cycle transcriptomics revises *Leishmania mexicana* genome annotation and links a chromosome duplication with parasitism of vertebrates. *PLoS Pathog.* **11**, e1005186. doi:10.1371/journal.ppat.1005186

Fu, G., Wang, Q., Phan, N., Urbanska, P., Joachimiak, E., Lin, J., Wloga, D. and Nicastro, D. (2018). The I1 dynein-associated tether and tether head complex is a conserved regulator of ciliary motility. *Mol. Biol. Cell* **29**, 1048-1059. doi:10.1091/mbc.E18-02-0142

Gadelha, C., Wickstead, B., McKean, P. G. and Gull, K. (2006). Basal body and flagellum mutants reveal a rotational constraint of the central pair microtubules in the axonemes of trypanosomes. *J. Cell Sci.* **119**, 2405-2413. doi:10.1242/jcs.02969

Gomelsky, M. and Klug, G. (2002). BLUF: a novel FAD-binding domain involved in sensory transduction in microorganisms. *Trends Biochem. Sci.* **27**, 497-500. doi:10.1016/S0968-0004(02)02181-3

Harrison, A., Olds-Clarke, P. and King, S. M. (1998). Identification of the t complex-encoded cytoplasmic dynein light chain tctex1 in inner arm I1 supports the involvement of flagellar dyneins in meiotic drive. *J. Cell Biol.* **140**, 1137-1147. doi:10.1083/jcb.140.5.1137

Hendrickson, T. W., Perrone, C. A., Griffin, P., Wuichet, K., Mueller, J., Yang, P., Porter, M. E. and Sale, W. S. (2004). IC138 is a WD-repeat dynein intermediate chain required for light chain assembly and regulation of flagellar bending. *Mol. Biol. Cell* **15**, 5431-5442. doi:10.1091/mbc.e04-08-0694

Hendrickson, T. W., Goss, J. L., Seaton, C. A. and Rohrs, H. W. (2013). The IC138 and IC140 intermediate chains of the I1 axonemal dynein complex bind directly to tubulin. *Biochim. Biophys. Acta* **1833**, 3265-3271. doi:10.1016/j.bbamcr.2013.09.011

Heuser, T., Raytchev, M., Krell, J., Porter, M. E. and Nicastro, D. (2009). The dynein regulatory complex is the nexin link and a major regulatory node in cilia and flagella. *J. Cell Biol.* **187**, 921-933. doi:10.1083/jcb.200908067

Heuser, T., Barber, C. F., Lin, J., Krell, J., Rebesco, M., Porter, M. E. and Nicastro, D. (2012). Cryoelectron tomography reveals doublet-specific structures and unique interactions in the I1 dynein. *Proc. Natl. Acad. Sci. USA* **109**, E2067-E2076. doi:10.1073/pnas.1120690109

Hoog, J. L., Gluenz, E., Vaughan, S. and Gull, K. (2010). Ultrastructural investigation methods for Trypanosoma brucei. *Methods Cell Biol.* **96**, 175-196. doi:10.1016/S0091-679X(10)96008-1

Huang, B., Ramanis, Z. and Luck, D. J. (1982). Suppressor mutations in Chlamydomonas reveal a regulatory mechanism for flagellar function. *Cell* **28**, 115-124. doi:10.1016/0092-8674(82)90381-6

Ikeda, K., Yamamoto, R., Wirschell, M., Yagi, T., Bower, R., Porter, M. E., Sale, W. S. and Kamiya, R. (2009). A novel ankyrin-repeat protein interacts with the regulatory proteins of inner arm dynein f (I1) of Chlamydomonas reinhardtii. *Cell Motil. Cytoskeleton* **66**, 448-456. doi:10.1002/cm.20324

Iseki, M., Matsunaga, S., Murakami, A., Ohno, K., Shiga, K., Yoshida, K., Sugai, M., Takahashi, T., Hori, T. and Watanabe, M. (2002). A blue-light-activated adenylyl cyclase mediates photoavoidance in Euglena gracilis. *Nature* **415**, 1047-1051. doi:10.1038/4151047a

Kato-Minoura, T., Hirono, M. and Kamiya, R. (1997). Chlamydomonas inner-arm dynein mutant, ida5, has a mutation in an actin-encoding gene. *J. Cell Biol.* **137**, 649-656. doi:10.1083/jcb.137.3.649

Kelley, L. A., Mezulis, S., Yates, C. M., Wass, M. N. and Sternberg, M. J. (2015). The Phyre2 web portal for protein modeling, prediction and analysis. *Nat. Protoc.* **10**, 845-858. doi:10.1038/nprot.2015.053

King, S. M. (2018). Turning dyneins off bends cilia. *Cytoskeleton (Hoboken)* **75**, 372-381. doi:10.1002/cm.21483

Krausz, C., Escamilla, A. R. and Chianese, C. (2015). Genetics of male infertility: from research to clinic. *Reproduction* **150**, R159-R174. doi:10.1530/REP-15-0261

Kubo, T., Hou, Y., Cochran, D. A., Witman, G. B. and Oda, T. (2018). A microtubule-dynein tethering complex regulates the axonemal inner dynein f (I1). *Mol. Biol. Cell* **29**, 1060-1074. doi:10.1091/mbc.E17-11-0689

Lechtreck, K. F. and Witman, G. B. (2007). Chlamydomonas reinhardtii hydin is a central pair protein required for flagellar motility. *J. Cell Biol.* **176**, 473-482. doi:10.1083/jcb.200611115

Li, H. and Durbin, R. (2009). Fast and accurate short read alignment with Burrows-Wheeler transform. *Bioinformatics* **25**, 1754-1760. doi:10.1093/bioinformatics/btp324

Li, H., Handsaker, B., Wysoker, A., Fennell, T., Ruan, J., Homer, N., Marth, G., Abecasis, G., Durbin, R. and Genome Project Data Processing Subgroup. (2009). The sequence alignment/map format and SAMtools. *Bioinformatics* **25**, 2078-2079. doi:10.1093/bioinformatics/btp352

Lin, J. and Nicastro, D. (2018). Asymmetric distribution and spatial switching of dynein activity generates ciliary motility. *Science* **360**, eaar1968. doi:10.1126/science.aar1968

Lindemann, C. B. and Lesich, K. A. (2010). Flagellar and ciliary beating: the proven and the possible. *J. Cell Sci.* **123**, 519-528. doi:10.1242/jcs.051326

Masuda, S. and Bauer, C. E. (2002). AppA is a blue light photoreceptor that antirepresses photosynthesis gene expression in Rhodobacter sphaeroides. *Cell* **110**, 613-623. doi:10.1016/S0092-8674(02)00876-0

Mitchison, H. M. and Valente, E. M. (2017). Motile and non-motile cilia in human pathology: from function to phenotypes. *J. Pathol.* **241**, 294-309. doi:10.1002/path.4843

Myster, S. H., Knott, J. A., O'Toole, E. and Porter, M. E. (1997). The Chlamydomonas Dhc1 gene encodes a dynein heavy chain subunit required for assembly of the I1 inner arm complex. *Mol. Biol. Cell* **8**, 607-620. doi:10.1091/mbc.8.4.607

Myster, S. H., Knott, J. A., Wysocki, K. M., O'Toole, E. and Porter, M. E. (1999). Domains in the 1alpha dynein heavy chain required for inner arm assembly and flagellar motility in Chlamydomonas. *J. Cell Biol.* **146**, 801-818. doi:10.1083/jcb.146.4.801

Neto, F. T., Bach, P. V., Najari, B. B., Li, P. S. and Goldstein, M. (2016). Genetics of male infertility. *Curr. Urol. Rep.* **17**, 70. doi:10.1007/s11934-016-0627-x

Oda, T., Yanagisawa, H. and Kikkawa, M. (2015). Detailed structural and biochemical characterization of the nexin-dynein regulatory complex. *Mol. Biol. Cell* **26**, 294-304. doi:10.1091/mbc.E14-09-1367

Okutman, O., Rhouma, M. B., Benkhalifa, M., Muller, J. and Viville, S. (2018). Genetic evaluation of patients with non-syndromic male infertility. *J. Assist. Reprod. Genet.* **35**, 1939-1951. doi:10.1007/s10815-018-1301-7

Perrone, C. A., Yang, P., O'Toole, E., Sale, W. S. and Porter, M. E. (1998). The Chlamydomonas IDA7 locus encodes a 140-kDa dynein intermediate chain required to assemble the I1 inner arm complex. *Mol. Biol. Cell* **9**, 3351-3365. doi:10.1091/mbc.9.12.3351

Piperno, G. (1990). Functional diversity of dyneins. *Cell Motil. Cytoskeleton* **17**, 147-149. doi:10.1002/cm.970170302

Porter, M. E., Power, J. and Dutcher, S. K. (1992). Extragenic suppressors of paralyzed flagellar mutations in Chlamydomonas reinhardtii identify loci that alter the inner dynein arms. *J. Cell Biol.* **118**, 1163-1176. doi:10.1083/jcb.118.5.1163

Ralston, K. S. and Hill, K. L. (2006). Trypanin, a component of the flagellar Dynein regulatory complex, is essential in bloodstream form African trypanosomes. *PLoS Pathog.* **2**, e101. doi:10.1371/journal.ppat.0020101

Reiter, J. F. and Leroux, M. R. (2017). Genes and molecular pathways underpinning ciliopathies. *Nat. Rev. Mol. Cell Biol.* **18**, 533-547. doi:10.1038/nrm.2017.60

Robinson, D. R. and Gull, K. (1991). Basal body movements as a mechanism for mitochondrial genome segregation in the trypanosome cell cycle. *Nature* **352**, 731-733. doi:10.1038/352731a0

Robinson, J. T., Thorvaldsdóttir, H., Winckler, W., Guttman, M., Lander, E. S., Getz, G. and Mesirov, J. P. (2011). Integrative genomics viewer. *Nat. Biotechnol.* **29**, 24-26. doi:10.1038/nbt.1754

Schindelin, J., Arganda-Carreras, I., Frise, E., Kaynig, V., Longair, M., Pietzsch, T., Preibisch, S., Rueden, C., Saalfeld, S., Schmid, B. et al. (2012). Fiji: an open-source platform for biological-image analysis. *Nat. Methods* **9**, 676-682. doi:10.1038/nmeth.2019

Sievers, F., Wilm, A., Dineen, D., Gibson, T. J., Karplus, K., Li, W., Lopez, R., McWilliam, H., Remmert, M., Söding, J. et al. (2011). Fast, scalable generation of high-quality protein multiple sequence alignments using Clustal Omega. *Mol. Syst. Biol.* **7**, 539. doi:10.1038/msb.2011.75

Smith, E. F. and Sale, W. S. (1991). Microtubule binding and translocation by inner dynein arm subtype I1. *Cell Motil. Cytoskeleton* **18**, 258-268. doi:10.1002/cm.970180403

Tang, S., Wang, X., Li, W., Yang, X., Li, Z., Liu, W., Li, C., Zhu, Z., Wang, L., Wang, J. et al. (2017). Biallelic mutations in CFAP43 and CFAP44 cause male infertility with multiple morphological abnormalities of the sperm flagella. *Am. J. Hum. Genet.* **100**, 854-864. doi:10.1016/j.ajhg.2017.04.012

Toba, S., Fox, L. A., Sakakibara, H., Porter, M. E., Oiwa, K. and Sale, W. S. (2011). Distinct roles of 1alpha and 1beta heavy chains of the inner arm dynein I1 of Chlamydomonas flagella. *Mol. Biol. Cell* **22**, 342-353. doi:10.1091/mbc.e10-10-0806

Trudgian, D. C., Thomas, B., McGowan, S. J., Kessler, B. M., Salek, M. and Acuto, O. (2010). CPFP: a central proteomics facilities pipeline. *Bioinformatics* **26**, 1131-1132. doi:10.1093/bioinformatics/btq081

Trudgian, D. C., Ridlova, G., Fischer, R., Mackeen, M. M., Ternette, N., Acuto, O., Kessler, B. M. and Thomas, B. (2011). Comparative evaluation of label-free SINQ normalized spectral index quantitation in the central proteomics facilities pipeline. *Proteomics* **11**, 2790-2797. doi:10.1002/pmic.201000800

Urbanska, P., Joachimiak, E., Bazan, R., Fu, G., Poprzeczko, M., Fabczak, H., Nicastro, D. and Wloga, D. (2018). Ciliary proteins Fap43 and Fap44 interact with each other and are essential for proper cilia and flagella beating. *Cell. Mol. Life Sci.* **75**, 4479-4493. doi:10.1007/s00018-018-2819-7

VanderWaal, K. E., Yamamoto, R., Wakabayashi, K.-I., Fox, L., Kamiya, R., Dutcher, S. K., Bayly, P. V., Sale, W. S. and Porter, M. E. (2011). bop5 Mutations reveal new roles for the IC138 phosphoprotein in the regulation of flagellar motility and asymmetric waveforms. *Mol. Biol. Cell* **22**, 2862-2874. doi:10.1091/mbc.e11-03-0270

Viswanadha, R., Hunter, E. L., Yamamoto, R., Wirschell, M., Alford, L. M., Dutcher, S. K. and Sale, W. S. (2014). The ciliary inner dynein arm, I1 dynein, is assembled in the cytoplasm and transported by IFT before axonemal docking. *Cytoskeleton (Hoboken)* **71**, 573-586. doi:10.1002/cm.21192

Vizcaíno, J. A., Csordas, A., Del-Toro, N., Dianes, J. A., Griss, J., Lavidas, I., Mayer, G., Perez-Riverol, Y., Reisinger, F., Ternent, T. et al. (2016). 2016 update of the PRIDE database and its related tools. *Nucleic Acids Res.* **44**, 11033. doi:10.1093/nar/gkw880

Wheeler, R. J. (2017). Use of chiral cell shape to ensure highly directional swimming in trypanosomes. *PLoS Comput. Biol.* **13**, e1005353. doi:10.1371/journal.pcbi.1005353

Wheeler, R. J., Gluenz, E. and Gull, K. (2011). The cell cycle of Leishmania: morphogenetic events and their implications for parasite biology. *Mol. Microbiol.* **79**, 647-662. doi:10.1111/j.1365-2958.2010.07479.x

Wheeler, R. J., Gluenz, E. and Gull, K. (2015). Basal body multipotency and axonemal remodelling are two pathways to a 9+0 flagellum. *Nat. Commun.* **6**, 8964. doi:10.1038/ncomms9964

Williams, B. D., Velleca, M. A., Curry, A. M. and Rosenbaum, J. L. (1989). Molecular cloning and sequence analysis of the Chlamydomonas gene coding for radial spoke protein 3: flagellar mutation pf-14 is an ochre allele. *J. Cell Biol.* **109**, 235-245. doi:10.1083/jcb.109.1.235

Wiśniewski, J. R., Zougman, A., Nagaraj, N. and Mann, M. (2009). Universal sample preparation method for proteome analysis. *Nat. Methods* **6**, 359-362. doi:10.1038/nmeth.1322

Yamamoto, R., Song, K., Yanagisawa, H. A., Fox, L., Yagi, T., Wirschell, M., Hirono, M., Kamiya, R., Nicastro, D. and Sale, W. S. (2013). The MIA complex is a conserved and novel dynein regulator essential for normal ciliary motility. *J. Cell Biol.* **201**, 263-278. doi:10.1083/jcb.201211048

Yang, P., Yang, C. and Sale, W. S. (2004). Flagellar radial spoke protein 2 is a calmodulin binding protein required for motility in Chlamydomonas reinhardtii. *Eukaryot. Cell* **3**, 72-81. doi:10.1128/EC.3.1.72-81.2004

Yang, P., Diener, D. R., Yang, C., Kohno, T., Pazour, G. J., Dienes, J. M., Agrin, N. S., King, S. M., Sale, W. S., Kamiya, R. et al. (2006). Radial spoke proteins of Chlamydomonas flagella. *J. Cell Sci.* **119**, 1165-1174. doi:10.1242/jcs.02811